Significance of Hydrogen Bonding Network in the Proton-Coupled Electron Transfer Reactions of Photosystem II from a Quantum-Mechanical Perspective

Journal:	*Physical Chemistry Chemical Physics*
Manuscript ID	CP-ART-02-2019-000868.R1
Article Type:	Paper
Date Submitted by the Author:	29-Mar-2019
Complete List of Authors:	Chai, Jun; Shanghai Institute of Ceramics Chinese Academy of Sciences, Zheng, Zhaoyang; Chinese Academy of Engineering Physics, ; Pan, Hui; University of Macao, Institute of Applied Physics and Materials Engineering; University of Macau, Department of Physics and Chemistry Zhang, Shengbai; Rensselaer Polytechnic Institute, Lakshmi, K. V.; Rensselaer Polytechnic Institute, Chemistry and Chemical Biology Sun, Yi-Yang; Shanghai Institute of Ceramics, Chinese Academy of Sciences, State Key Lab of High Performance Ceramics and Superfine Microstructure

PCCP

ARTICLE

Significance of Hydrogen Bonding Network in the Proton-Coupled Electron Transfer Reactions of Photosystem II from a Quantum-Mechanical Perspective

Received 00th January 20xx,
Accepted 00th January 20xx

DOI: 10.1039/x0xx00000x

www.rsc.org/

Jun Chai,[a] Zhaoyang Zheng,[b] Hui Pan,[c] Shengbai Zhang,[d] K. V. Lakshmi*,[e] and Yi-Yang Sun*,[a]

The photosynthetic protein complex, photosystem II (PSII), conducts the light-driven water-splitting reaction with unrivaled efficiency. Proton-coupled electron transfer (PCET) reactions at the redox-active tyrosine residues are thought to play a critical role in the water-splitting chemistry. Addressing the fundamental question as to why the tyrosine residue, Y_Z, is kinetically competent in comparison with a symmetrically placed tyrosine residue, Y_D, is important for the elucidation of the mechanism of PCET in the water-splitting reaction of PSII. Here, using all-quantum-mechanical calculations we study PCET at the Y_Z and Y_D residues of PSII. We find that when Y_Z is in its protein matrix under physiological conditions, the HOMO of Y_Z constitutes the HOMO of the whole system. In contrast, the HOMO of Y_D is buried under the electronic states localized elsewhere in the protein matrix and PCET at Y_D requires the transfer of the phenolic proton, which elevates the HOMO of Y_D to being the HOMO of the whole system. This leads to the oxidation of Y_D albeit on a slower timescale. Our study reveals that the key differences in the electronic structure of Y_Z and Y_D is primarily determined by the protonation state of the respective hydrogen-bonding partners, D1-His190 and D2-His189, or more generally by the H-bonding network of the protein matrix.

Introduction

Photosystem II (PSII), a photosynthetic protein complex in the thylakoid membranes of plants, algae, and cyanobacteria, catalyzes one of the most energetically demanding reactions in nature by using solar energy to drive the catalytic oxidation of water to dioxygen.[1-4] Light-driven proton-coupled electron transfer (PCET) reactions, which are exquisitely tuned by smart protein matrix effects and hydrogen (H)-bonded water molecules, are central to the water-splitting chemistry of PSII.[5-11] Elucidating the water-splitting chemistry of PSII is of intense interest as it supports life on Earth. Moreover, it is important to determine the mechanism of the water-splitting reaction in PSII as it is a blueprint for the design of a new generation of bio-inspired catalytic systems for solar fuel production.[12-21] In recent years, the high-resolution X-ray crystal structures of PSII[22-29] have presented an exciting opportunity to elucidate the mechanism of the light-driven PCET reactions that lead to the highly-efficient water-splitting chemistry of PSII.

Shown in Figure 1a is the X-ray crystal structure of the PSII dimer at 1.9 Å resolution.[28, 29] The light-driven primary electron transport occurs in the heterodimeric polypeptide core (regions marked by yellow frames) on each monomer. The cofactors that are involved in the primary electron-transfer pathway are shown in Figure 1b. The photochemistry is initiated by the absorption of light through the antenna complexes which leads to photoexcitation and charge separation at the special chlorophylls, P_{680}. This creates the charge-separated P_{680}^+-$Pheo_A^-$ state, where the hole is transported to the catalytic Mn_4Ca-oxo cluster[30] in the oxygen-evolving complex (OEC) while the electron is transferred to the secondary plastoquinone acceptor, Q_B. Four iterations of the photoexcitation and charge separation reaction result in the oxidation of two molecules of water to dioxygen and the generation of reducing equivalents in the form of plastoquinol (Q_BH_2) that are subsequently used for CO_2 fixation.

The primary electron transfer pathway of PSII involves two symmetrically placed redox-active tyrosine residues, Y_Z and Y_D, one on each subunit of the core polypeptides, D1 and D2, respectively (Figure 1b).[28, 29, 31-33] The function of these tyrosine residues is quite distinct as the smart protein matrix effects influence tyrosine redox function in PSII. While Y_Z is kinetically competent and directly participates in the water-splitting reaction,[1, 34, 35] it is proposed that the Y_D redox poises the catalytic Mn_4Ca-oxo cluster[36] and may be involved in the secondary electron transfer pathway of PSII.[37, 38] Both Y_Z and Y_D undergo light-driven PCET, however, these residues have distinct properties that include differences in the time scales and

[a] State Key Laboratory of High Performance Ceramics and Superfine Microstructure, Shanghai Institute of Ceramics, Chinese Academy of Sciences, Shanghai 201899, China. Email: yysun@mail.sic.ac.cn
[b] National Key Laboratory of Shock Wave and Detonation Physics, Institute of Fluid Physics, China Academy of Engineering Physics, Mianyang 621900, China.
[c] Joint Key Laboratory of the Ministry of Education, Institute of Applied Physics and Materials Engineering, University of Macau, Taipa, Macao SAR 999078, China.
[d] Department of Physics, Applied Physics, and Astronomy, Rensselaer Polytechnic Institute, Troy, NY, 12180, USA.
[e] Department of Chemistry and Chemical Biology and The Baruch '60 Center for Biochemical Solar Energy Research, Rensselaer Polytechnic Institute, Troy, NY, 12180, USA. Email: lakshk@rpi.edu
† Electronic Supplementary Information (ESI) available

specificity of redox activity. To date, the factors that influence the functional tuning of these cofactors remain under debate.

In this study, we use all quantum-mechanical (all-QM) calculations based on density-functional theory (DFT) to elucidate the mechanism of light-driven PCET. The all-QM approach presents a powerful tool to investigate the tuning of the Y_Z and Y_D residues at the electronic structure level and determine the polypeptide-cofactor interactions that lead to the distinct redox properties. The PCET reactions of PSII have previously been addressed by hybrid QM/MM approaches.[39, 40] The protonation state of the Y_Z and its conjugate base, the histidine-190 residue in the D1 polypeptide (D1-His190), has been shown to depend on pH.[39] Other studies have also suggested that pH and microsolvation could influence the redox activity and proton transfer of both Y_Z and Y_D.[33, 41-43] The all-QM calculations allow us to investigate the relative alignment of the energy levels of the Y_Z and Y_D orbitals relative to other components of the whole system, which is inaccessible by QM/MM approaches. As revealed in this work, such alignments provide critical insight on the functional differences between Y_Z and Y_D. In order to elucidate the effects of the protein matrix on the electronic structure of Y_Z and Y_D, we construct PSII models that are comprised of approx. 800 atoms including the respective redox-active tyrosine residue (Y_Z or Y_D), its conjugate base (the His-190 and His189 residue in the D1 and D2 polypeptide, respectively) and all of the neighboring amino acid residues. We demonstrate that there is a difference in the energy levels of the frontier orbitals of the Y_Z and Y_D residues within the overall electronic structure of each protein model. Our all-QM calculations reveal that the H-bonding network within the protein matrix determines the protonation state of the D1-His190 and D2-His189 residues, which in turn tunes the energy levels of the frontier orbitals of Y_Z and Y_D.

Methods

This study was based on density functional theory (DFT) with the generalized gradient approximation of Perdew, Burke and Ernzerhof (PBE)[44] for the exchange-correlation functional, as implemented in the VASP program.[45] Projector augmented wave (PAW) potentials[46] were used to describe the core-valence interaction and plane-waves up to kinetic energy of 340 eV were used as the basis set. The models containing Y_Z or Y_D and their respective molecular environments were placed in periodic supercells, where the spacing between the repeating images were separated by a vacuum region of ~ 6 Å. The Brillouin zone of the reciprocal space was represented by the Γ point at the zone center and spin-polarized calculations were employed in this study. We compared the computed eigenvalue positions of amino acids by the plane-wave PAW method with those obtained by localized Gaussian basis sets to test the accuracy of the calculations which is presented in the Supporting Information.

The coordinates for the heavy atoms in this study were derived from the recent X-ray crystal structure of PSII at 1.9 Å resolution (PDB ID: 3ARC).[28] The model for Y_Z is comprised of three segments of the D1 polypeptide containing the residues D1-Phe155-Asp170, D1-Asn181-His195, and D1-Ile290-Phe300, respectively, the Mn_4Ca-oxo cluster and side chains of D1-His332, D1-Glu333, D1-His337, D1-Asp342, D1-Ala344, CP43-Glu354 and CP43-Arg357. Seven water molecules in the vicinity of Y_Z (W1-W7[47] or W358, W428, W540, W541, W542, W999, and W1000 in the naming convention used the PDB file, 3ARC) were also included in the model. The Y_Z model contains 818 atoms (or 819 atoms with the D1-His190 residue in the protonated state).

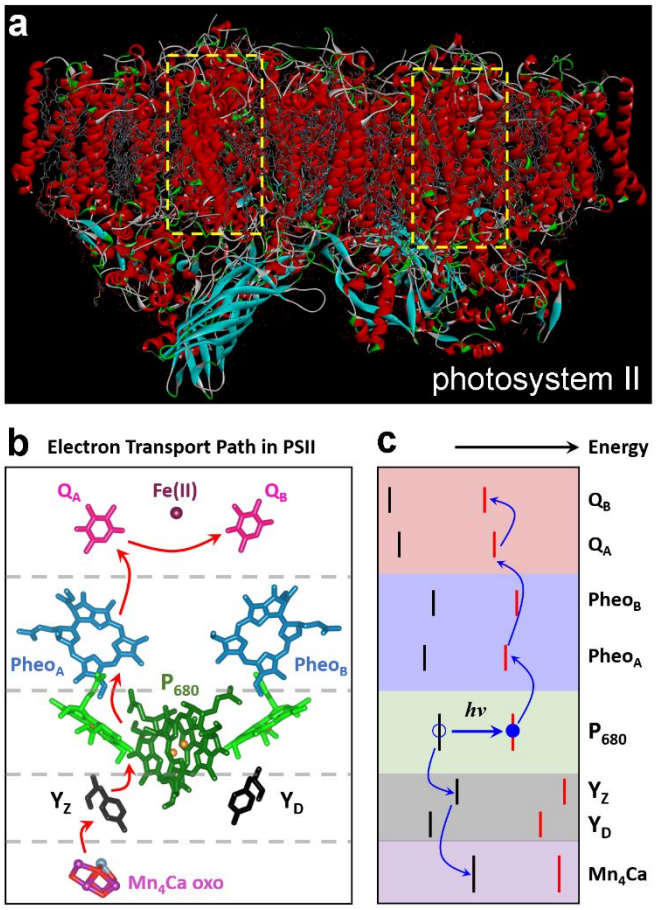

Figure 1 (a) The X-ray crystal structure of the PSII dimer at 1.9 Å resolution (Ref. 28). The yellow frames mark the heterodimeric polypeptide core where the light-driven electron transport occurs. (b) A view of the highlighted regions in part (a) that depict the electron-transfer cofactors of PSII. The red arrows indicate the primary electron transfer pathway. (c) An energy-level diagram illustrating the alignment of the HOMO and LUMO states of the cofactors. Blue arrows depict electron and hole transport following charge separation at the special chlorophylls, P_{680}.

Since 3d transition metal oxides are well-known strongly-correlated systems, we employed the DFT+*U* approach to describe the Mn 3d orbitals of the Mn_4Ca-oxo cluster in the OEC.[48] We used a *U* value of 5 eV that is derived from first-

principles calculations of MnO.[49] Upon optimizing the electronic structure of the neutral Y_Z residue using a DFT+*U* functional, we obtain a total magnetic moment of 14 μ_B for the Mn_4Ca-oxo cluster with two of the manganese ions contributing ~ 4 μ_B each and the other two manganese ions contributing ~ 3 μ_B each. This is consistent with the S_1 state of the Mn_4Ca-oxo cluster that is comprised of two Mn(III) and two Mn(IV) ions.[50] We find that as long as the Y_Z orbital is not buried by the 3d orbitals of the manganese ions of the Mn_4Ca-oxo cluster, the results are not sensitive to the value of *U* that is used in the calculations.

The model for Y_D was comprised of three segments in the D2 polypeptide containing residues D2-Val154-Ala170, D2-Arg180-Asn194, and D2-Val286-Tyr296, respectively, and a short segment from the CP47 polypeptide containing the residues CP47-Ala361, CP47-Phe362, and CP47-Phe363. The sole water molecule with double occupancy in the 1.9 Å X-ray crystal structure[28] was included in the model. The Y_D model contains 780 atoms (or 779 atoms with the D2-His189 residue in the unprotonated state).

In both the Y_Z and Y_D models, the amino acid residues were selected such that the H-bonded tyrosine-histidine couple was encapsulated by an extensive protein matrix. The initial coordinates of hydrogen atoms were generated using the *reduce* code[51] and then optimized in the DFT calculations. The coordinates of the side chains of the tyrosine-histidine couple, the Mn_4Ca-oxo cluster and water molecules were also optimized in the calculations and the optimization was performed until the atomic forces were smaller than 0.05 eV/Å. The protonation state of the histidine was varied in the different Y_Z and Y_D models. The extra charge that was introduced upon protonation of the histidine was balanced by a uniform counter charge distributed on the whole supercell, which a technique that is commonly used with the periodic boundary condition.[52]

Results

The Effect of the Protein Matrix on the Atomic Structure of Y_Z. Initially, we consider the neutral state of the Y_Z residue with the surrounding protein matrix, Mn_4Ca-oxo cluster and water molecules. This allows us to investigate the effect of the protein matrix on the electronic structure to gain critical insight on the mechanism of PCET at the Y_Z residue. The key features of the model are the (i) protonation state of Y_Z and its H-bonding partner, D1-His190, (ii) distance between the two residues and (iii) H-bonded network of water molecules in the vicinity of Y_Z. Figure 2a-b shows the optimized core regions of the Y_z model. In the neutral state, the phenolic oxygen of Y_Z is protonated. There are two possibilities for the protonation state of D1-His190 where the N_ε atom is either deprotonated (referred to as model A or Y_Z-A) or protonated (referred to as model B or Y_Z-B). We optimized the atomic structures of both of the models. Also shown in Figure 2a-b are the minimum energy H-bonding configurations of the water molecules, W1-W7, in the Y_Z-A and Y_Z-B model, respectively.

We observe that the distance between the phenolic O atom of Y_Z (denoted as O_Z) and the N_ε atom of D1-His190 in the optimized model Y_Z-A is 2.48 Å which is an unusually short H-bond. This is in excellent agreement with the X-ray crystal structure of PSII where the O_Z-N_ε distance is 2.46 Å.[26, 28] The H atom of the phenolic group of Y_Z (denoted as H_Z) in the Y_Z-A model is nearly equidistant between O_Z and N_ε and there are no metastable positions for the H_Z atom in the vicinity of O_Z and N_ε in this model. In contrast, the O_Z-N_ε distance in the Y_Z-B model is longer at 2.67 Å and the H_Z atom is interacting with the water molecule W4 (Figure 2b) which is a consequence of the protonation of the N_ε atom on D1-His190 residue. We also assess the effect of the H-bonding network of water molecules on the structure of Y_Z in both models. We find that upon removing five water molecules (W3-W7) in the vicinity of Y_Z, the O_Z-N_ε distance increases from 2.48 Å to 2.66 Å in the Y_Z-A model and 2.67 Å to 2.83 Å in the Y_Z-B model. These results indicate that the unusually short O_Z-N_ε distance and hence the strong interaction between Y_Z and D1-His190 is due to the combined effect of the deprotonated N_ε atom on D1-His190 and the presence of a network of H-bonded water molecules in the vicinity of Y_Z. Our calculations estimate that each individual effect contributes to a reduction of about 0.2 Å in the O_Z-N_ε distance.

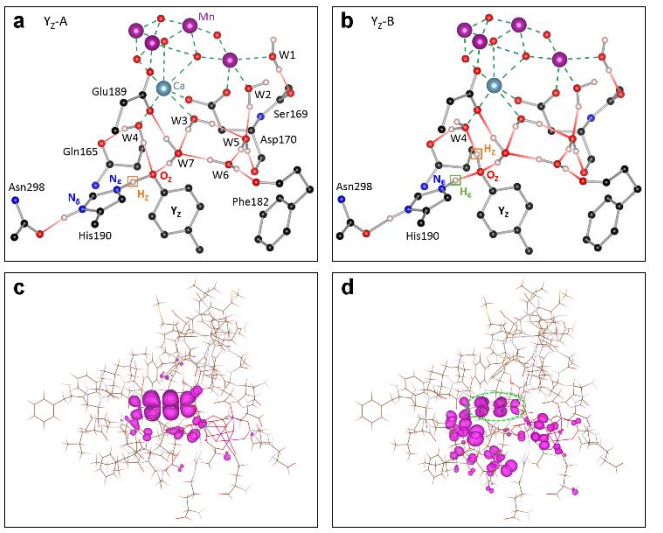

Figure 2 Atomic structure of Y_Z in (a) model A and (b) model B. The C, N, O, and H atoms are shown in black, blue, red, and pink, respectively. For clarity, only the core regions of the models are shown here and the H atoms that are not involved in the H-bonding network are omitted in this figure. In Y_Z-A, the H atom H_Z, as marked by a brown-colored square, is shared by the N_ε atom of D1-His190 and the O_Z atom of Y_Z. In Y_Z-B, H_Z is oriented towards a water molecule (W4), while an extra H atom (H_ε), as marked by a green square, is bonded to the N_ε atom of D1-His190. The H-bonds are shown by lines of gradient color. Parts (c) and (d) show the charge density distribution in the HOMO state of Y_Z in model Y_Z-A and Y_Z-B, respectively. While the orbitals in Y_Z-A are localized on Y_Z, the orbitals highlighted by a green circle in part (d) indicate that the position of the Y_Z orbitals in Y_Z-B are mixed amongst other orbitals in the computational model.

The Effect of the Protein Matrix on the Electronic Structure of Y_Z. As demonstrated in the previous section, the atomic structure of the Y_Z residue in the Y_Z-A and Y_Z-B models is in agreement with the X-ray crystal structures and previous theoretical investigations, respectively.[26, 28, 39] In this section, we investigate the effect of the protein matrix on the electronic structure of Y_Z. As an accurate depiction of the surrounding matrix, we have simultaneously included the Mn_4Ca-oxo cluster, water molecules and neighboring amino acid residues in a single QM model (Figure 2a-b). Moreover, the amino acids are connected through the polypeptide backbone to minimize the effect of terminating bonds.

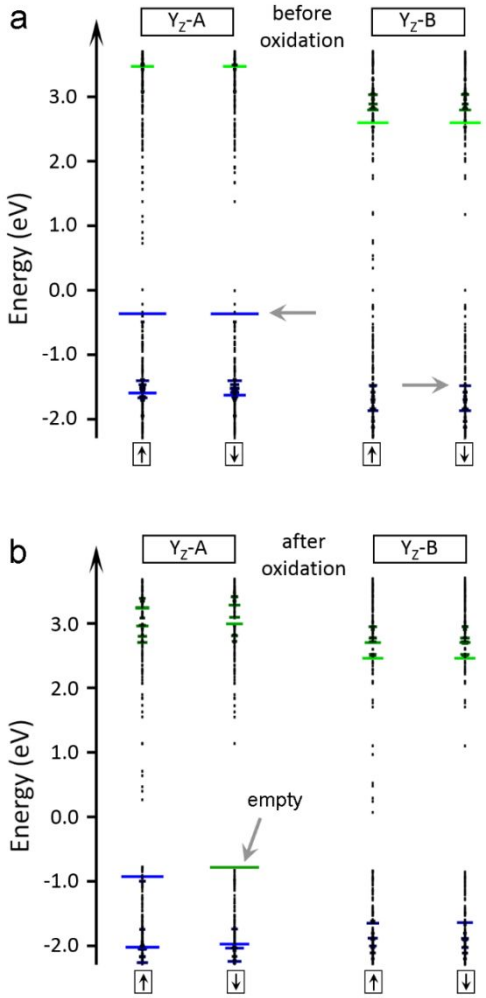

Figure 3 The eigenvalue spectra of the Y_Z-A and Y_Z-B model (a) before and (b) after oxidation. The spin up and spin down components are marked by an up and down arrow in each frame, respectively. Each horizontal bar represents an eigenstate and the width of the bar represents the projection of the state on the side-chain atoms of Y_Z. Thus, a wider bar indicates a larger projection. A state with no projection on Y_Z appears as a black dot. The occupied and unoccupied Y_Z states are shown in blue and green, respectively. The arrows in part (a) mark the HOMO states of Y_Z in A and B models. The corresponding charge density plots are shown in Figure 2c-d, respectively. The hole (or empty) state created by oxidation of Y_Z-A is marked by an arrow in part (b). The position of the HOMO level prior to oxidation is chosen as the reference energy (i.e., energy zero).

Shown in Figure 3a is a comparison of the eigenvalue spectra of the Y_Z residue in the Y_Z-A and Y_Z-B model. The horizontal bars represent the projection of a particular eigenstate on the atoms of the Y_Z residue. The blue and green bars represent the occupied and unoccupied molecular orbitals that are localized on Y_Z, respectively. We observe a significant difference between the electronic structure of the Y_Z-A and Y_Z-B model. In the Y_Z-A model, the highest occupied molecular orbital (HOMO) of Y_Z (marked by an arrow in Figure 3a) is close to the HOMO of the whole system at reference energy of zero. In contrast, the HOMO of Y_Z in the Y_Z-B model is buried by the electronic states that are localized on other amino acid residues and/or the protein backbone. Moreover, the projection of the eigenvalues on Y_Z, as represented by the width of the horizontal bar in Figure 3a, in the Y_Z-B model is much smaller than the projection in Y_Z-A. This indicates that the Y_Z state in the Y_Z-B model is significantly mixed with orbitals localized on other parts of the system. The charge densities of the HOMO of Y_Z in the Y_Z-A and Y_Z-B model are shown in Figure 2c-d, respectively, where the HOMO of Y_Z is predominately localized on Y_Z in the Y_Z-A model, while it is significantly mixed with orbitals that are localized on other amino acid residues in the Y_Z-B model.

The difference in the electronic structure of Y_Z-A and Y_Z-B is further evident when examining the oxidized state of each model. We calculate the eigenvalue spectra for both models by oxidizing the system by one electron. As seen in Figure 3b, the HOMO of Y_Z in the Y_Z-A model contains an empty orbital upon oxidation of the spin-down component signaling that the hole is localized on Y_Z. This indicates that Y_Z is the primary electron donor in the Y_Z-A model. Furthermore, we observe that in the oxidized state of Y_Z-A the proton H_Z is displaced from being evenly shared between the O_Z and N_ε atoms to a position in which it is bonded solely to the N_ε atom with a N_ε-H_Z bond length of 1.09 Å and an increase in the O_Z-N_ε distance from 2.48 Å to 2.56 Å. This suggests that the one-electron oxidation of Y_Z induces the transfer of a proton from Y_Z to its conjugate base, D1-His190. These results indicate that PCET at Y_Z in the Y_Z-A model involves electron transfer accompanied by the transfer of a proton. The displacement of the phenolic proton, H_Z, that is observed here is consistent with a previous study of PCET intermediates of tyrosine using pulsed electron nuclear double resonance (ENDOR) spectroscopy.[53, 54] A previous theoretical study has reported that in the oxidized state, H_Z can also be bound to the O_Z atom in a metastable configuration.[39] However, we do not observe a metastable configuration in the present study.

In contrast to Y_Z-A, oxidation does not affect the atomic and electronic structure of Y_Z in the Y_Z-B model. As shown in Figure 3b, there are no states near the HOMO of the system that are localized on Y_Z. This suggests that the hole that is created upon the oxidation of the system is not localized on the Y_Z residue. This is consistent with the observation that prior to oxidation the HOMO of Y_Z in the Y_Z-B model is buried under other electronic states that are not localized on Y_Z (Figure 3a).

The Effect of the Protein Matrix on Y_D. As demonstrated in the previous section, the protonation state of the conjugate base, D1-His190, has a critical impact on the electronic structure of Y_Z. Here, we investigate the effect of the different protonation states of the conjugate base, D2-His189, on the electronic structure of the Y_D residue. There is an important difference in the environment of D2-His189 in comparison with D1-His190, namely, the N_δ atom of D2-His189 is H-bonded to a protonated N atom of D2-Arg294 (Figure 4). Thus, under physiological conditions the D2-His189 residue is protonated at the N_ε site (model A or Y_D-A). In addition, we also consider the possibility that the N_ε atom of D2-His189 is deprotonated in model B or Y_D-B (here both the N_δ and N_ε atoms of D2-His189 are in a deprotonated state).

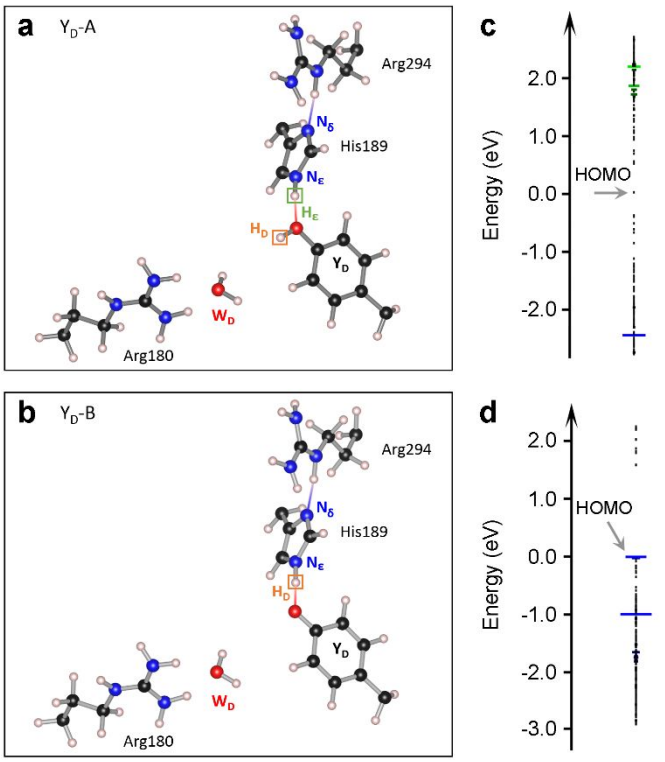

Figure 4 Atomic structure of the (a) Y_D-A and (b) Y_D-B model. The C, N, O, and H atoms are shown in black, blue, red, and pink, respectively. For clarity, only the core regions of the models are shown. The sole water molecule in the vicinity of Y_D is denoted by W_D, while the H atom of the phenolic group of Y_D is denoted by H_D. The positions of H_D are highlighted by brown squares and the H_ε atom is marked by a green square. The H-bonds are shown by lines of gradient color. Parts (c) and (d) depict the eigenvalue spectra of the Y_D-A and Y_D-B model, respectively.

Shown in Figure 4a-b is the optimized atomic structure of the core regions of Y_D-A and Y_D-B model in the neutral state. While there is uncertainty in the position of the water molecule, W_D, in the X-ray crystal structure of PSII,[28] we find that its impact on the electronic structure of Y_D is negligible. However, the protonation state of the conjugate base, D2-His189, has a major influence on the redox activity of Y_D. Shown in Figure 4c-d are the eigenvalue spectra of the Y_D-A and Y_D-B model in the neutral state, where each electronic state is projected on to the Y_D residue. We observe that the HOMO of Y_D in the Y_D-B model is at a much higher energy than it is in Y_D-A, which suggests that Y_D in the Y_D-B model is an active electron donor in PSII. The effect of protonation of the conjugate base in the Y_D-B model is similar to that of Y_Z in the Y_Z-A model in that the H_D (or H_Z) atom is positioned between Y_D (or Y_Z) and the N_ε atom of D2-His189 (or D1-His190).

Upon oxidization of the Y_D-B model, we observe that the hole of the whole system is localized on Y_D and the H_D atom is transferred from the phenolic O_D atom of Y_D to the N_ε atom of D2-His189. This observation is similar to the oxidation of Y_Z in the Y_Z-A model in that oxidation at Y_D is accompanied by the transfer of a proton. However, it should be noted that the O_D-N_ε donor-acceptor distance of 2.57 Å for Y_D in Y_D-B is longer than the O_Z-N_ε distance of 2.48 Å for Y_Z in the Y_Z-A model, which could be due to the absence of an extensive network of H-bonded water molecules in the vicinity of Y_D. This is important as it suggests that the redox kinetics of Y_D, even in the relatively active Y_D-B model would be slower than that of Y_Z in the Y_Z-A model.[55] This is in agreement with experimental observations of the kinetics of PCET at the Y_D and Y_Z residues of PSII,[53, 56] as well as QM/MM simulations.[40]

Discussion

When the respective residue is in the protein matrix, the HOMO of the whole system may or may not be localized on Y_Z or Y_D as the electronic structure of the tyrosine is subject to tuning by the protein matrix. Our results demonstrate that the HOMO of the tyrosine could be buried by the orbitals localized on the side chains of other amino acid residues or the backbone states of the polypeptide, which would render it unresponsive to the oxidation process. In fact, it is not *a priori* that a tyrosine residue should serve as the electron donor to P_{680}^+ in the protein matrix. We calculated the energy levels of the HOMO and LUMO of 20 amino acids *in vacuo* that are shown in Figure 5. The energy of the HOMO of a tyrosine residue is not the highest; in fact there are five amino acids that have HOMO energies that are either comparable to or higher than that of a tyrosine residue. However, when the residue undergoes PCET the displacement of the phenolic proton increases the energy of the HOMO of the tyrosine to above the other occupied orbitals such that it serves as the HOMO of the whole system.

Based on the all-QM calculations, the redox activity of the Y_Z and Y_D residue of PSII is strongly correlated with the protonation state of the respective conjugate base, D1-His190 and D2-His189, respectively. If we consider the histidine residue with a single protonated N atom (either N_ε or N_δ), that is physiologically relevant, then the A models for Y_Z and Y_D correspond to this state. However, the electronic structures of Y_Z-A and Y_D-A are distinctly different. In Y_Z-A, the HOMO of Y_Z behaves as a frontier orbital and upon oxidation an electron is transferred from the HOMO of Y_Z. In contrast, the HOMO of Y_D

in the Y_D-A model is buried under other states that are localized on neighboring amino acid residues. This difference provides a consistent understanding to the distinct redox activities of Y_Z and Y_D under physiological conditions, where Y_Z is kinetically competent while the oxidation of Y_D is slow. However, as has been previously reported the rate of oxidation of Y_D becomes comparable to that of Y_Z when the pH is higher than 8.5.[41] This is because at pH values above the pKa of histidine, D2-His189 can be deprotonated at both the N_δ and N_ϵ sites, converting Y_D from model Y_D-A to model Y_D-B, which behaves comparable to Y_Z-A. Similarly, under strongly acidic conditions, Y_Z can be converted from the Y_Z-A to Y_Z-B model by protonation of both the N_δ and N_ϵ atoms of D1-His190 such that the redox activity is inhibited.[33, 43]

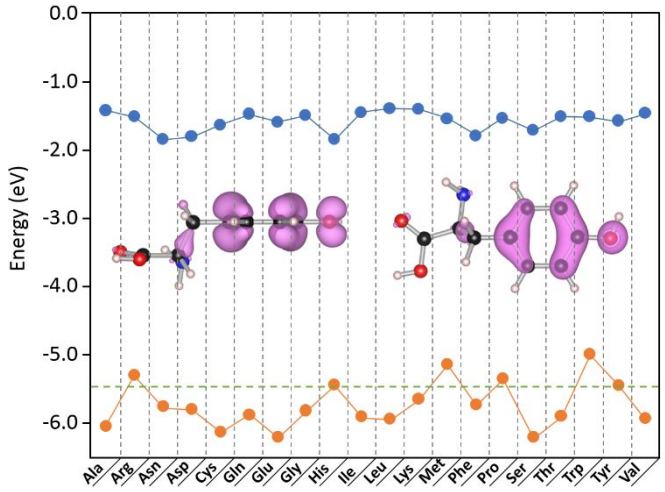

Figure 5 The calculated energies of the HOMO (brown) and LUMO (blue) states of 20 amino acid residues in vacuo. The dashed line marks the energy of the HOMO of tyrosine. The inset depicts the side (left) and top (right) views of the charge density distribution in the HOMO of tyrosine, which are compared with those in Figure 2c-d.

Thus, while the redox activity of Y_Z and Y_D is determined by the conjugate base, D1-His190 or D2-His189, the protonation states of the conjugate base is in turn determined by the alternate H-bond partners. The N_δ atom of D1-His190 is H-bonded to the O atom of D1-Asn298 (Figure 2a-b). Since the latter is not protonated, it allows for the N_δ atom of D1-His190 to be in a protonated state. Thus, the N_ϵ atom of D1-His190 is deprotonated in the physiological state which leads to the A model of Y_Z. In contrast, the N_δ atom of D2-His189 is H-bonded to one of the N atoms in the side chain of D2-Arg294 (Figure 4). Since the latter is protonated, it allows for the N_δ atom of D2-His189 to be deprotonated. As a result, in the physiological state N_ϵ of D2-His189 is protonated which leads to the A model of Y_D.

Conclusions

In summary, we have performed an all-QM study of the redox-active tyrosine residues, Y_Z and Y_D, of PSII. Our calculations reproduce the key structural parameters of the recent high-resolution X-ray crystal structure of PSII.[28] We observe that the energy level of the HOMO of Y_Z and Y_D in the overall electronic structure of the protein matrix provides important insight on the mechanism of PCET at each residue. In particular, under physiological conditions the Y_Z orbital constitutes the frontier orbital of the whole system, which ensures rapid electron transfer followed by proton transfer i.e. an ET/PT reaction. In contrast, under physiological conditions the Y_D orbital is buried underneath states that are localized on other amino acids in the system which decreases the rate of electron transfer. This difference in the electronic structure of Y_Z and Y_D is the result of a difference in the protonation state of the respective conjugate base, D1-His190 and D2-His189, which in turn is determined by the hydrogen-bonding network in the protein matrix. The methods that are applied in this study are highly applicable to the study of proton-coupled electron transfer reactions in other photosynthetic and respiratory proteins.

Acknowledgements

Y.Y.S. acknowledges support by the National Natural Science Foundation of China under Grant number 11774365. S.B.Z. acknowledges support by NSF under Grant DMREF-1627028. K.V.L. acknowledges support by the US Department of Energy, Office of Science, Photosynthetic Systems Program under the contract DE-FG02-07ER15903. S. B. Z. acknowledges the use of Extreme Science and Engineering Discovery Environment (XSEDE), which is supported by National Science Foundation grant number ACI-1548562.

Notes and references

1. J. P. McEvoy and G. W. Brudvig, *Chemical Reviews*, 2006, **106**, 4455-4483.
2. M. M. Najafpour, G. Renger, M. Holynska, A. N. Moghaddam, E. M. Aro, R. Carpentier, H. Nishihara, J. J. Eaton-Rye, J. R. Shen and S. I. Allakhverdiev, *Chemical Reviews*, 2016, **116**, 2886-2936.
3. J. R. Shen, *Annual Review of Plant Biology*, 2015, **66**, 23-48.
4. D. G. Nocera, *Accounts of Chemical Research*, 2012, **45**, 767-776.
5. M. H. V. Huynh and T. J. Meyer, *Chemical Reviews*, 2007, **107**, 5004-5064.
6. T. J. Meyer, M. H. V. Huynh and H. H. Thorp, *Angewandte Chemie-International Edition*, 2007, **46**, 5284-5304.
7. B. A. Barry, *Nature Chemistry*, 2014, **6**, 376-377.
8. A. Migliore, N. F. Polizzi, M. J. Therien and D. N. Beratan, *Chemical Reviews*, 2014, **114**, 3381-3465.
9. M. Suga, F. Akita, M. Sugahara, M. Kubo, Y. Nakajima, T. Nakane, K. Yamashita, Y. Umena, M. Nakabayashi, T. Yamane, T. Nakano, M. Suzuki, T. Masuda, S. Inoue, T. Kimura, T. Nomura, S. Yonekura, L. J. Yu, T. Sakamoto, T. Motomura, J. H. Chen, Y. Kato, T. Noguchi, K. Tono, Y. Joti, T. Kameshima, T. Hatsui, E. Nango, R. Tanaka, H. Naitow, Y. Matsuura, A. Yamashita, M. Yamamoto, O. Nureki, M. Yabashi, T. Ishikawa, S. Iwata and J. R. Shen, *Nature*, 2017, **543**, 131--135.
10. J. Kern, R. Chatterjee, I. D. Young, F. D. Fuller, L. Lassalle, M. Ibrahim, S. Gul, T. Fransson, A. S. Brewster, R. Alonso-Mori, R. Hussein, M. Zhang, L. Douthit, C. de Lichtenberg, M. H. Cheah, D. Shevela, J. Wersig, I. Seuffert, D. Sokaras, E. Pastor, C. Weninger, T. Kroll, R. G. Sierra, P. Aller, A. Butryn, A. M. Orville, M. N. Liang, A. Batyuk, J. E. Koglin, S. Carbajo, S. Boutet, N. W. Moriarty, J. M. Holton, H. Dobbek, P. D. Adams, U. Bergmann, N. K. Sauter, A. Zouni, J. Messinger, J. Yano and V. K. Yachandra, *Nature*, 2018, **563**, 421-425.
11. A. J. Wilson and P. K. Jain, *Journal of the American Chemical Society*, 2018, **140**, 5853-5859.
12. F. E. Osterloh, *Chemistry of Materials*, 2008, **20**, 35-54.
13. D. Gust, T. A. Moore and A. L. Moore, *Accounts of Chemical Research*, 2009, **42**, 1890-1898.
14. J. Barber, *Chemical Society Reviews*, 2009, **38**, 185-196.

15. J. D. Megiatto Jr, D. D. Méndez-Hernández, M. E. Tejeda-Ferrari, A.-L. Teillout, M. J. Llansola-Portolés, G. Kodis, O. G. Poluektov, T. Rajh, V. Mujica, T. L. Groy, D. Gust, T. A. Moore and A. L. Moore, *Nature Chemistry*, 2014, **6**, 423-428.
16. R. G. Hadt, D. Hayes, C. N. Brodsky, A. M. Ullmann, D. M. Casa, M. H. Upton, D. G. Nocera and L. X. Chen, *Journal of the American Chemical Society*, 2016, **138**, 11017-11030.
17. C. X. Zhang, C. H. Chen, H. X. Dong, J. R. Shen, H. Dau and J. Q. Zhao, *Science*, 2015, **348**, 690-693.
18. E. Romero, V. I. Novoderezhkin and R. van Grondelle, *Nature*, 2017, **543**, 355-365.
19. E. Odella, S. J. Mora, B. L. Wadsworth, M. T. Huynh, J. J. Goings, P. A. Liddell, T. L. Groy, M. Gervaldo, L. E. Sereno, D. Gust, T. A. Moore, G. F. Moore, S. Hammes-Schiffer and A. L. Moore, *Journal of the American Chemical Society*, 2018, **140**, 15450-15460.
20. K. P. Sokol, W. E. Robinson, J. Warnan, N. Kornienko, M. M. Nowaczyk, A. Ruff, J. Z. Zhang and E. Reisner, *Nature Energy*, 2018, **3**, 944-951.
21. G. Maayan, N. Gluz and G. Christou, *Nature Catalysis*, 2018, **1**, 48-54.
22. A. Zouni, H. T. Witt, J. Kern, P. Fromme, N. Krauss, W. Saenger and P. Orth, *Nature*, 2001, **409**, 739-743.
23. N. Kamiya and J. R. Shen, *Proceedings of the National Academy of Sciences of the United States of America*, 2003, **100**, 98-103.
24. K. N. Ferreira, T. M. Iverson, K. Maghlaoui, J. Barber and S. Iwata, *Science*, 2004, **303**, 1831-1838.
25. A. Guskov, J. Kern, A. Gabdulkhakov, M. Broser, A. Zouni and W. Saenger, *Nature Structural & Molecular Biology*, 2009, **16**, 334-342.
26. F. H. M. Koua, Y. Umena, K. Kawakami and J. R. Shen, *Proceedings of the National Academy of Sciences of the United States of America*, 2013, **110**, 3889-3894.
27. I. D. Young, M. Ibrahim, R. Chatterjee, S. Gul, F. D. Fuller, S. Koroidov, A. S. Brewster, R. Tran, R. Alonso-Mori, T. Kroll, T. Michels-Clark, H. Laksmono, R. G. Sierra, C. A. Stan, R. Hussein, M. Zhang, L. Douthit, M. Kubin, C. de Lichtenberg, L. V. Pham, H. Nilsson, M. H. Cheah, D. Shevela, C. Saracini, M. A. Bean, I. Seuffert, D. Sokaras, T. C. Weng, E. Pastor, C. Weninger, T. Fransson, L. Lassalle, P. Brauer, P. Aller, P. T. Docker, B. Andi, A. M. Orville, J. M. Glownia, S. Nelson, M. Sikorski, D. L. Zhu, M. S. Hunter, T. J. Lane, A. Aquila, J. E. Koglin, J. Robinson, M. N. Liang, S. Boutet, A. Y. Lyubimov, M. Uervirojnangkoorn, N. W. Moriarty, D. Liebschner, P. V. Afonine, D. G. Waterman, G. Evans, P. Wernet, H. Dobbek, W. I. Weis, A. T. Brunger, P. H. Zwart, P. D. Adams, A. Zouni, J. Messinger, U. Bergmann, N. K. Sauter, J. Kern, V. K. Yachandra and J. Yano, *Nature*, 2016, **540**, 453-457.
28. Y. Umena, K. Kawakami, J. R. Shen and N. Kamiya, *Nature*, 2011, **473**, 55-60.
29. M. Suga, F. Akita, K. Hirata, G. Ueno, H. Murakami, Y. Nakajima, T. Shimizu, K. Yamashita, M. Yamamoto, H. Ago and J. R. Shen, *Nature*, 2015, **517**, 99-103.
30. J. Yano and V. Yachandra, *Chemical Reviews*, 2014, **114**, 4175-4205.
31. D. Koulougliotis, X. S. Tang, B. A. Diner and G. W. Brudvig, *Biochemistry*, 1995, **34**, 2850-2856.
32. A. W. Rutherford, A. Boussac and P. Faller, *Biochimica Et Biophysica Acta-Bioenergetics*, 2004, **1655**, 222-230.
33. S. Styring, J. Sjoholm and F. Mamedov, Biochimica Et Biophysica Acta-Bioenergetics, 2012, **1817**, 76-87.
34. J. P. McEvoy and G. W. Brudvig, *Physical Chemistry Chemical Physics*, 2004, **6**, 4754-4763.
35. J. S. Vrettos, J. Limburg and G. W. Brudvig, *Biochimica Et Biophysica Acta-Bioenergetics*, 2001, **1503**, 229-245.
36. S. Styring and A. W. Rutherford, *Biochemistry*, 1987, **26**, 2401-2405.
37. C. A. Tracewell and G. W. Brudvig, *Biochemistry*, 2003, **42**, 9127-9136.
38. B. A. Diner and F. Rappaport, *Annual Review of Plant Biology*, 2002, **53**, 551-580.
39. K. Saito, J. R. Shen, T. Ishida and H. Ishikita, *Biochemistry*, 2011, **50**, 9836-9844.
40. K. Saito, A. W. Rutherford and H. Ishikita, *Proceedings of the National Academy of Sciences of the United States of America*, 2013, **110**, 7690-7695.
41. P. Faller, R. J. Debus, K. Brettel, M. Sugiura, A. W. Rutherford and A. Boussac, *Proceedings of the National Academy of Sciences of the United States of America*, 2001, **98**, 14368-14373.
42. A. Sirohiwal, F. Neese and D. A. Pantazis, *Journal of the American Chemical Society*, 2019, **141**, 3217-3231.
43. R. Ahlbrink, M. Haumann, D. Cherepanov, O. Bogershausen, A. Mulkidjanian and W. Junge, *Biochemistry*, 1998, **37**, 1131-1142.
44. J. P. Perdew, K. Burke and M. Ernzerhof, *Physical Review Letters*, 1996, **77**, 3865-3868.
45. G. Kresse and J. Furthmüller, *Computational Materials Science*, 1996, **6**, 15-50.
46. G. Kresse and D. Joubert, *Physical Review B*, 1999, **59**, 1758-1775.
47. K. Kawakami, Y. Umena, N. Kamiya and J. R. Shen, *Journal of Photochemistry and Photobiology B-Biology*, 2011, **104**, 9-18.
48. S. L. Dudarev, G. A. Botton, S. Y. Savrasov, C. J. Humphreys and A. P. Sutton, *Physical Review B*, 1998, **57**, 1505-1509.
49. B.-C. Shih, T. A. Abtew, X. Yuan, W. Zhang and P. Zhang, *Physical Review B*, 2012, **86**, 165124.
50. T. Kuntzleman and C. F. Yocum, *Biochemistry*, 2005, **44**, 2129-2142.
51. J. M. Word, S. C. Lovell, J. S. Richardson and D. C. Richardson, *Journal of Molecular Biology*, 1999, **285**, 1735-1747.
52. C. Freysoldt, B. Grabowski, T. Hickel, J. Neugebauer, G. Kresse, A. Janotti and C. G. Van de Walle, *Reviews of Modern Physics*, 2014, **86**, 253-305.
53. R. Chatterjee, C. S. Coates, S. Milikisiyants, C.-I. Lee, A. Wagner, O. G. Poluektov and K. V. Lakshmi, *Biochemistry*, 2013, **52**, 4781-4790.
54. J. D. Megiatto, D. D. Mendez-Hernandez, M. E. Tejeda-Ferrari, A. L. Teillout, M. J. Llansola-Portoles, G. Kodis, O. G. Poluektov, T. Rajh, V. Mujica, T. L. Groy, D. Gust, T. A. Moore and A. L. Moore, *Nature Chemistry*, 2014, **6**, 423-428.
55. M. T. Zhang, T. Irebo, O. Johansson and L. Hammarstrom, *Journal of the American Chemical Society*, 2011, **133**, 13224-13227.
56. S. Nakamura and T. Noguchi, *Biochemistry*, 2015, **54**, 5045-5053.

TOC Graphic

All quantum-mechanical calculations provide insights into the effect of hydrogen bonding network on the proton-coupled electron transfer at Y_Z and Y_D in photosystem II.